



Universidad Autónoma  
de Madrid

**Biblos-e Archivo**  
Repositorio Institucional UAM

**Repositorio Institucional de la Universidad Autónoma de Madrid**

<https://repositorio.uam.es>

Esta es la **versión de autor** del artículo publicado en:  
This is an **author produced version** of a paper published in:

Physical Chemistry Chemical Physics 23.36 (2021): 20174-20182

**DOI:** <https://doi.org/10.1039/d1cp02055b>

**Copyright:** © the Owner Societies 2021

El acceso a la versión del editor puede requerir la suscripción del recurso  
Access to the published version may require subscription

Cite this: DOI: 00.0000/xxxxxxxxxx

# Imaging intramolecular hydrogen migration with time- and momentum-resolved photoelectron diffraction<sup>†</sup>

Fukiko Ota,<sup>a</sup> Shigeru Abe,<sup>a</sup> Keisuke Hatada,<sup>a,‡</sup> Kiyoshi Ueda,<sup>b,\*</sup> Sergio Díaz-Tendero,<sup>c,d,e,¶</sup> and Fernando Martín<sup>c,d,f,§</sup>

Received Date

Accepted Date

DOI: 00.0000/xxxxxxxxxx

Imaging ultrafast hydrogen migration with few- or sub-femtosecond time resolution is a challenge for ultrafast spectroscopy due to the lightness and small scattering cross section of the moving hydrogen atom. Here we propose time- and momentum-resolved photoelectron diffraction (TMR-PED) as a way to overcome limitations of existing methodologies and illustrate its performance in the ethanol molecule. By combining different theoretical methods, namely molecular dynamics and electron scattering methods, we show that TMR-PED, along with a judicious choice of the reference frame for multicoincidence detection, allows for direct imaging of single and double hydrogen migration in doubly-charged ethanol with both few-fs and Ångström resolutions, all the way from its birth to the very end. It also provides hints of proton extraction following H<sub>2</sub> roaming. The signature of hydrogen dynamics shows up in polarization-averaged molecular-frame photoelectron angular distributions (PA-MFPADs) as moving features that allow for a straightforward visualization in space.

## 1 Introduction

Real-time imaging of few-femtosecond structural changes in molecules is a long-standing dream of chemical sciences<sup>1,2</sup>, as it can provide unprecedented insight on ultrafast chemical reactions. Access to this ultrashort time scale is nowadays possible by using table-top attosecond and few-femtosecond laser pulses (from IR to soft X-rays)<sup>3–5</sup> or, more recently, X-ray free-electron laser (XFEL) pulses<sup>4,6</sup>. However, imaging few-Å structural changes with such a high temporal resolution is still extremely challenging and requires the development of more advanced visualization tools. For example, a MeV ultrafast electron diffraction (UED) system<sup>7</sup> developed at SLAC in 2015 permitted

to observe structural changes in extended two-dimensional materials and nanoparticles with hundred μm and hundred fs resolutions. Further improvements of this technique have led to a significant gain in spatial resolution, down to the Å limit, as in a recent study of the photochemical ring-opening in cyclohexadiene<sup>8</sup>. A similar gain in spatial resolution has also been achieved by using X-ray pulses generated at XFELs. Indeed, due to their high brightness, diffractive scattering of XFEL pulses is orders of magnitude more efficient than that of X-ray light produced by more conventional sources (e.g., synchrotrons), thus allowing for structural molecular imaging<sup>9,10</sup>, even at the single-molecule level<sup>11</sup>.

Though successful, these approaches are rather insensitive to the motion of hydrogen atoms due to their low scattering cross sections. Hydrogen (proton) migration is, however, one of the most fundamental reactions occurring in physical, chemical and biological environments<sup>12–16</sup>. So far, real-time information on hydrogen migration has been obtained by using two, rather indirect, imaging methods. The first one is time-resolved Coulomb explosion imaging (CEI), where the momenta of all ions resulting from the fragmentation of a single doubly-ionized molecule are detected as a function of the delay between the pump and the probe pulses produced by an intense laser. In CEI, one assumes a one-to-one correspondence between the kinetic energy of the released fragments and the time these fragments took to separate from each other before the probe pulse arrives, thus providing the desired temporal information. This method has been successfully employed to extract temporal information on hydrogen migration

<sup>a</sup> Department of Physics, University of Toyama, Gofuku 3190, Toyama 930-8555, Japan

<sup>b</sup> Department of Chemistry, Tohoku University, 6-3 Aramaki Aza-Aoba, Aoba-ku, Sendai 980-8578, Japan

<sup>c</sup> Departamento de Química, Módulo 13, Universidad Autónoma de Madrid, 28049 Madrid, Spain, EU

<sup>d</sup> Condensed Matter Physics Center (IFIMAC), Universidad Autónoma de Madrid, 28049 Madrid, Spain, EU

<sup>e</sup> Institute for Advanced Research in Chemical Sciences (IAChem), Universidad Autónoma de Madrid, 28049 Madrid, Spain, EU

<sup>f</sup> Instituto Madrileño de Estudios Avanzados en Nanociencia (IMDEA-Nano), Campus de Cantoblanco, 28049 Madrid, Spain, EU

<sup>†</sup> Electronic Supplementary Information (ESI) available: [details of any supplementary information available should be included here]. See DOI: 00.0000/00000000.

<sup>‡</sup> hatada@sci.u-toyama.ac.jp

<sup>\*</sup> kiyoshi.ueda@tohoku.ac.jp

<sup>¶</sup> sergio.diaztendero@uam.es

<sup>§</sup> fernando.martin@uam.es

occurring in the isomerization of acetylene to vinylidene<sup>17–20</sup>, in acetonitrile<sup>21</sup> and ethanol<sup>22</sup>, and, very recently, on hydrogen roaming in formaldehyde<sup>23</sup>. Extracting spatial information from CEI is, however, not straightforward and very often impossible.

The second method is laser-induced electron diffraction (LIED)<sup>24</sup>, where an electron resulting from tunnel ionization returns to the molecule driven by the strong laser field and then diffracts providing a spatial image of the molecule with sub-Å resolution. The temporal information is retrieved from the measurement of the full momentum of the diffracted electron. LIED is sensitive to hydrogen atoms because it involves relatively low-energy electrons (50 – 100 eV) in comparison with those used in UED (megavolts). Thus, this technique has not only been successful in probing structural changes associated with the motion of heavier atoms, as in molecular oxygen<sup>24</sup> and OCS<sup>25</sup>, but also with those associated to hydrogen migration, as in water<sup>26</sup> and acetylene<sup>27</sup>. However, as the nuclear dynamics probed by LIED is that occurring during the round trip of the electron, i.e., during an optical cycle of the driving laser, temporal imaging is mostly limited to the very early stages of the migration process, usually well before the hydrogen atoms have reached their final destination.

In this work, we show, by combining different theoretical methods, that an alternative route to image hydrogen migration that overcomes the above mentioned limitations is time- and momentum-resolved photoelectron diffraction (TMR-PED). PED has been shown to be sensitive to hydrogen atoms in several theoretical calculations and gas-phase synchrotron radiation experiments performed in a variety of molecular targets, such as methane<sup>28,29</sup>, water<sup>30</sup>, etc. It is also a well-established analysis tool in surface science<sup>31</sup>, where the energies and directions of core-level photoelectrons emitted from a specific site are measured relative to the sample orientation. To determine the full momentum of photoelectrons in gas-phase PED experiments, the molecular axis has to be fixed in space. This can be realized in so-called kinematically complete experiments, in which the momentum of ionic fragments is measured in coincidence with that of the photoelectrons by using, e.g., a COLTRIMS–Reaction Microscope<sup>32</sup>. We show that TMR-PED, in combination with a judicious choice of the reference frame for multicoincidence detection, allows for a direct imaging of single- (SHM) and double-hydrogen migration (DHM) in doubly-charged ethanol with both few-fs and Å resolutions, and provides hints of the more complex hydrogen roaming mechanism. And this all the way from the start to the end of the different processes ( $\sim 20$ ,  $\sim 50$  and  $\sim 60$  fs for SHM, DHM and roaming, respectively). The signature of the migrating hydrogen atoms shows up in the polarization-averaged molecular-frame photoelectron angular distributions (PA-MFPADs) as a moving feature that reflects the average trajectory followed by such atoms, thus allowing for a straightforward visualization of the dynamics in real space. Remarkably, this is the case after averaging over a statistical distribution of trajectories as that expected in a real experiment.

The dream of measuring TMR-PED<sup>33–35</sup> has now become feasible by using XFEL pulses<sup>36,37</sup> due to their high repetition-rate<sup>36</sup> and ultrashort duration (few-fs down to sub-fs)<sup>37</sup>. These pulses

are now at the disposal of users in several facilities. Kastirke *et al.*<sup>38,39</sup> have just reported the first successful implementation of this technique on the soft X-ray beam line of the European XFEL to image the dissociation dynamics of O<sub>2</sub>, and LCLS-II will soon start high repetition-rate operation in the soft to tender X-ray regions<sup>37</sup>. Furthermore, two-color XFEL operations, such as carbon 1s and oxygen 1s ionization, will be available at the European XFEL<sup>40</sup> and LCLS-II<sup>37</sup>. Therefore, the present study opens new avenues to record molecular movies, in particular of the often elusive intramolecular hydrogen migrations.

## 2 Theoretical modeling and choice of the relevant observables

To experimentally realize TMR-PED measurements that probe hydrogen motions in C<sub>2</sub>H<sub>5</sub>OH<sup>2+</sup>, two ultrashort X-ray pulses are needed. The first pulse (pump) to ionize either the C 1s or O 1s cores of neutral ethanol and produce dications via Auger decay, and the second pulse (probe) to generate the O 1s photoelectron for the PED measurement as a function of the pump-probe delay. We have chosen O 1s ionization in the probe step because ethanol only contains an oxygen atom and most migrating hydrogen atoms end up in the vicinity of oxygen. To measure the momentum of the electron ejected by the probe pulse, the 3D orientation of the molecule in space must be determined. For this, specific reaction channels must be selected from among all competing channels. To make this selection and identify the reaction plane, we employ channel-specific Coulomb explosion imaging (CEI) by the probe pulse. To simplify the atomic assignment in the experiment, one could use isotope labelled samples, as e.g. C<sub>2</sub>H<sub>5</sub>OD. However, since the basic concepts are the same for the non deuterated and deuterated species, and the dynamics is significantly slower (hence, more expensive) for the latter than for the former, we will only use non deuterated ethanol in our simulations. After interaction of doubly-charged ethanol with the X-ray probe pulse, the resulting triply-charged ethanol will further ionize as a result of Auger decay, thus leading to a quadruply-charged species that will finally break up into various (singly) charged fragments.

### 2.1 Theoretical methods

To reproduce the conditions found in a real experiment, we have performed Molecular Dynamics (MD) calculations on the ethanol dication with internal energy 10 eV for 1000 randomly chosen initial conditions (initial atomic momenta). The chosen values correspond to typical electronic excitation energies of dications generated via Auger decay. The underlying assumption is that, after Auger decay, the electronic excitation energy is rapidly transferred into the nuclear degrees of freedom (vibrational, rotational and kinetic) of the dication leading to the observed ionic fragments.

The MD simulations were carried out using the Atom Centered Density Matrix Propagation (ADMP) method<sup>41–43</sup>. In these simulations, the nuclei move classically in the potential computed on-the-fly with density functional theory (DFT), in particular with the B3LYP method<sup>44–46</sup> and the 6-31++G(d,p) basis set<sup>47–49</sup>. Prop-

agations were performed with a time step of  $\Delta t = 0.1$  fs and a fictitious electron mass of 0.1 amu, ensuring adiabaticity in the simulations. The starting point in the ADMP trajectories was the geometry of the two structural isomers of the neutral ethanol molecule, doubly ionized (Frank Condon transition), and considering a certain amount of excitation energy randomly redistributed over the nuclear degrees of freedom. We have computed 500 trajectories for each isomer. Relative energies corresponding to the ionization and relevant fragmentation channels have been computed at a high *ab initio* level of theory: Coupled Cluster including single, double and perturbative triple excitations<sup>50,51</sup> in combination with a correlation-consistent triple-Z basis set including polarization and diffuse functions<sup>52,53</sup>: CCSD(T)/aug-cc-pVTZ. Energies at this level of theory were computed over the geometry previously optimized with DFT-B3LYP/6-31++G(d,p). Relative energies are referred to the most stable neutral structure and are corrected using the zero-point-energy computed at the DFT-B3LYP/6-31++G(d,p) level. Molecular dynamics and potential energy surface calculations were performed using the Gaussian16 package<sup>54</sup>.

For all trajectories, the probabilities for O 1s photoionization of the dication by the probe pulse were evaluated by using the Multiple scattering theory<sup>55</sup> at selected time steps of the MD simulations. This theory uses a multi-center expansion in spherical harmonics together with numerical solution of the local Schrödinger equation on each atomic site. The scattering potentials are approximated by spherically symmetric ones, the so-called Muffin-tin approximation. To reduce computer time, we have used atomic **non self-consistent field (SCF)** electron densities<sup>56</sup>. We have checked the validity of this approximation by comparing at 0.1, 20 and 50 fs the resulting PA-MFPADs with those obtained by using the actual DFT electron density. The results are nearly indistinguishable. The real part of the Hedin-Lundqvist potential<sup>57,58</sup> is used as the optical potential. While the full multiple scattering scheme has been used for a photoelectron energy of 100 eV, a single scattering approximation has been used for 2.5 keV where its appropriateness was confirmed by a test calculation. The maximum values of the angular momentum,  $l_{\max}$ , for the partial wave expansion were 5, 5 and 4 for O, C, H for the 100 eV case. These values were estimated from the formula  $l_{\max} \sim kR_s$ , where  **$k$  is the momentum of the ejected electron and  $R_s$  is the Muffin-tin radius** obtained using the Norman criterium<sup>59</sup> without overlapping for the starting structure at 0 fs. The Muffin-tin radii and  $l_{\max}$  are fixed during the dynamics. For 2.5 keV, the values of  $l_{\max}$  obtained from the above formula are 17, 18 and 14 for O, C and H,

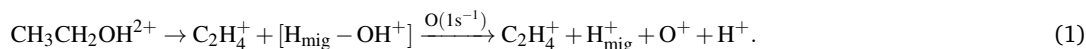
respectively. However, to save computation time, we have used  $l_{\max} = 10$  for all atoms, and we confirmed that the differences with the results obtained with the estimated values of  $l_{\max}$  were tiny. To obtain the PA-MFPADs, we took the sum of the three Cartesian components of the square modulus of the electric dipole matrix elements.<sup>60</sup> All the calculations have been performed by using the MsSpec code.<sup>61</sup>

It is worth noticing that PA-MFPADs have been calculated for intermediate ethanol dications that are far from the equilibrium geometry. This has been done for all trajectories leading to hydrogen migration and for a very large number of geometries per trajectory in order to get a smooth variation of the PA-MFPADs with the pump-probe delay. In this context, the use of the Multiple scattering method within the Muffin-tin approach has been found to be very convenient, as it is a relatively cheap approach in comparison with more sophisticated ones. However, this does not imply a significant loss of accuracy, since at the high photoelectron energies considered in this work, the photoelectron is not very sensitive to small details of the potential.

## 2.2 Choice of the relevant observables

In agreement with earlier work on doubly-charged ethanol<sup>22</sup>, the MD calculations show that single hydrogen migration is responsible for the production of  $\text{OH}_2^+$  ions through the reaction  $\text{CH}_3\text{CH}_2\text{OH}^{2+} \rightarrow \text{CH}_3\text{CH}^+ + \text{OH}_2^+$ , which involves the transfer of a hydrogen atom from the  $\text{CH}_3\text{CH}_2$  site to the OH site of the dication. The approximate yield of this process is  $\sim 1.0\%$ . Double-hydrogen migration leads to the production of  $\text{OH}_3^+$  ions through the reaction  $\text{CH}_3\text{CH}_2\text{OH}^{2+} \rightarrow \text{C}_2\text{H}_3^+ + \text{OH}_3^+$ , in which two hydrogen atoms jump from the  $\text{CH}_3\text{CH}_2$  site to the OH site of the dication, either sequentially or in a concerted manner. The yield of double-hydrogen migration is  $\sim 1.6\%$ . The MD calculations also show a non negligible production of  $\text{H}_3^+$  ions ( $\sim 1.7\%$  yield), which result from the formation of  $\text{H}_2$  through a roaming mechanism followed by extraction of a proton from the  $\text{C}_2\text{H}_3$  site by the roaming  $\text{H}_2$ . The relative energies of the different fragmentation channels are given in the Supplementary Material.

For the first H migration, we define the reaction plane as the plane containing the triangle whose vertices coincide with the centers of mass of  $\text{C}_2\text{H}_4^+$ ,  $\text{OH}^+$  (or  $\text{OD}^+$  for the isotope labelled molecule), and the first migrating hydrogen atom,  $\text{H}_{\text{mig}}$  (see Fig. 1a). O 1s ionization of the  $[\text{H}_{\text{mig}}-\text{OH}^+]$  complex by the probe pulse followed by Auger decay will lead to  $\text{H}_{\text{mig}}^+$ ,  $\text{O}^+$  and  $\text{H}^+$ . Thus, the full sequence of events while the first H atom is still migrating can be schematically represented



Therefore, experimentally the reaction plane must be determined by measuring the momentum correlation between  $\text{H}_{\text{mig}}^+$ ,  $\text{C}_2\text{H}_4^+$  and the sum of  $\text{O}^+$  and  $\text{H}^+$ . Note that two vectors are sufficient to define the plane.

For the second H migration, the reaction plane is defined by the triangle whose vertices coincide with the centers of mass of  $\text{C}_2\text{H}_3^+$ ,  $\text{OH}_2^+$ , and the second migrating hydrogen atom,  $\text{H}_{\text{mig}}$ . After O 1s ionization of the  $[\text{H}_{\text{mig}}-\text{OH}_2^+]$  complex by the probe pulse,  $\text{H}_{\text{mig}}^+$ ,

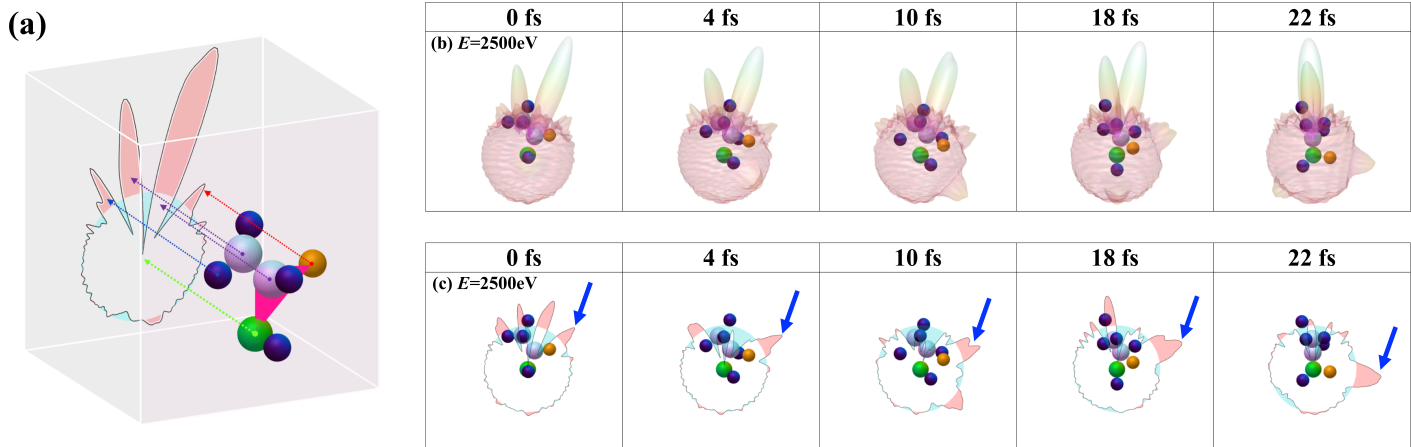
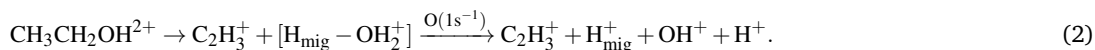


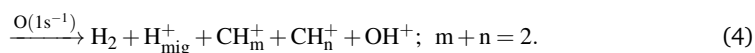
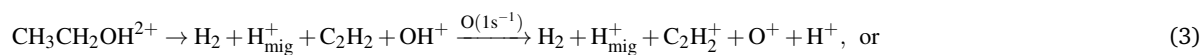
**Fig. 1** (a) Definition of the reaction plane in ethanol ( $\text{CH}_3\text{CH}_2\text{OH}$ ). For single-hydrogen migration, this plane contains the triangle (in pink color) whose vertices coincide with the centers of mass of the three fragments  $\text{C}_2\text{H}_4^+$ ,  $\text{OH}^+$ , and the first migrating H atom, and for double hydrogen migration,  $\text{C}_2\text{H}_3^+$ ,  $\text{OH}_2^+$  and the second migrating H atom. Color code for the different atoms: oxygen (green), carbon (white), migrating hydrogen atom (yellow) and other hydrogen atoms (blue). The panel also shows the projection of the PA-MFPAD in the chosen plane. (b) 3D PA-MFPADs as a function of the pump-probe delay for a single trajectory. The reaction plane has been rotated to overlap the plane on this page. (c) PA-MFPADs projected onto the reaction plane as a function of the pump-probe delay for a single trajectory. The light blue circle used as a reference in each panel has an area equal to the average intensity at 200 fs over the whole angular range. At this time, hydrogen migration is over. Peaks going beyond the circle limits are highlighted with red color. The blue arrows indicate the position of the peak associated with hydrogen migration in each time frame. The photoelectron energy in the three panels is 2.5 keV.

$\text{OH}^+$ , and  $\text{H}^+$  will be produced. In this case, the whole sequence of events while the second H atom is migrating is



Therefore, experimentally the reaction plane must be determined by measuring the momentum correlation between  $\text{H}_{\text{mig}}^+$ ,  $\text{C}_2\text{H}_3^+$  and the sum of  $\text{OH}^+$  and  $\text{H}^+$ .

The roaming of  $\text{H}_2$  with extraction of  $\text{H}_{\text{mig}}^+$  from  $\text{C}_2\text{H}_3^+$  to form  $\text{H}_3^+$  and the subsequent O 1s ionization proceeds through the following reactions



Thus, in the experiment, the reaction plane must be determined by measuring the momentum correlation between  $\text{H}_{\text{mig}}^+$ ,  $\text{C}_2\text{H}_2^+$  (or the sum of  $\text{CH}_m^+$  and  $\text{CH}_n^+$  with  $m + n = 2$ ) and the sum of  $\text{O}^+$  and  $\text{H}^+$  (or  $\text{OH}^+$ ).

For these selections of the reaction planes, we have obtained polarization-averaged molecular-frame photoelectron angular distributions, which are obtained by averaging over the three polarization directions the standard molecular-frame photoelectron angular distributions (MFPADs) for each molecular orientation. PA-MFPADs have been shown to mimic the molecular geometry more directly than MFPADs<sup>60,62–64</sup>.

### 3 Results and discussion

Fig. 1a shows, for a single trajectory, the PA-MFPAD for single-hydrogen migration in the corresponding reaction plane at a pump-probe delay of 0 fs (i.e., just after the formation of the doubly-charged ethanol ion). The chosen photoelectron energy is 2.5 keV. Figs. 1b and c show the time evolution of the calculated PA-MFPADs in full dimensionality and in the reaction plane, respectively. As can be seen, diffraction of the O 1s photoelectron by the different atomic centers leads to pronounced lobes or depletions with respect to a perfectly isotropic (spherical) distribution. Some of these features change as the different atoms move



### First hydrogen migration (SHM+DHM)

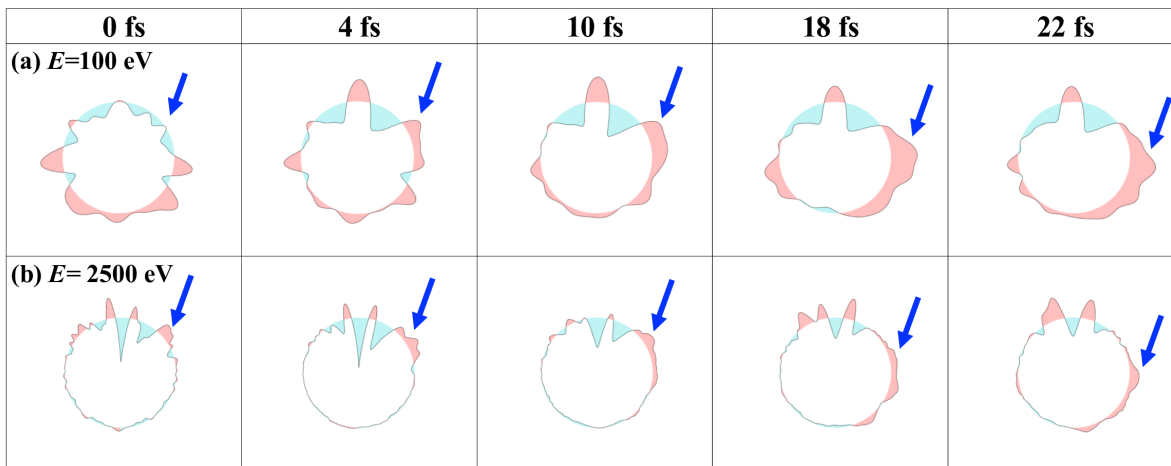


**Fig. 2** Snapshots of PA-MFPADs averaged over 26 trajectories for the first hydrogen migration ( $\leq 22$  fs) at photoelectron energies (a) 100 eV and (b) 2.5 keV. The blue arrows indicate the position of the peak associated with hydrogen migration in each time frame.

### Second hydrogen migration (DHM)

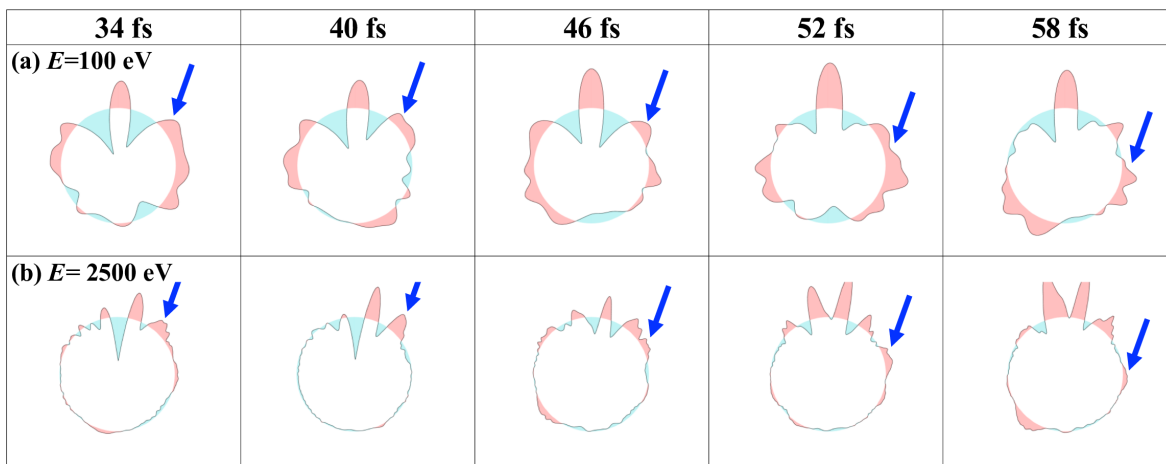


**Fig. 3** Snapshots of PA-MFPADs averaged over 16 trajectories for the second hydrogen migration (from 34 to 58 fs) at photoelectron energies (a) 100 eV and (b) 2.5 keV. The blue arrows indicate the position of the peak associated with hydrogen migration in each time frame.

with respect to the reaction plane, but those features associated with H migration closely follow the motion of the hydrogen atom. Therefore, for a fixed-in-space molecule with known orientation (as in the experimental realization described above), one can unambiguously associate the migration of the hydrogen atom to a specific moving feature in the PA-MFPAD and, hence, infer the trajectory followed by that atom and the time this atom needs to complete the different stages until it reaches its final destination, the OH molecular site.

A single trajectory, however, does not represent the real experimental situation, as the initial atomic positions and velocities are not unique, but rather follow a Wigner distribution around the equilibrium geometry. To account for this effect in the PA-MFPADs, we have performed a similar analysis for all trajectories leading to  $\text{OH}_2^+$  (single H migration) or  $\text{OH}_3^+$  (double H migration), irrespective of the initial conditions, and then performed a statistical average of the corresponding PA-MFPADs. The results for single- and double-hydrogen migration are shown in Figs. 2

and 3, respectively, for 100 eV and 2.5 keV photoelectron energies. The complete movies are given in the Supplementary Information. Although the average over different trajectories leading to the same  $\text{OH}_n^+$  fragment somewhat blurs the prominent features obtained for a single trajectory, hydrogen migrations can still be clearly identified by a feature that moves in a fairly similar way to a single trajectory (see Fig. 1c for the case of single hydrogen migration). Here it is important to emphasize that, due to our choice of the reaction planes and the multi-coincidence detection of the corresponding ionic fragments, which fixes molecular orientation, we minimize the dispersion of the calculated hydrogen migration paths. This low dispersion preserves the fingerprint of the process in the average PA-MFPADs. Our conclusions are valid for both single- and double-hydrogen migration, and at both low (100 eV) and high (2.5 keV) photoelectron energies, although the relevant features revealing the H motion are more apparent at higher energies. The total migration times,  $\sim 20$  fs and  $\sim 50$  fs for single- and double-hydrogen migration, respectively, are com-

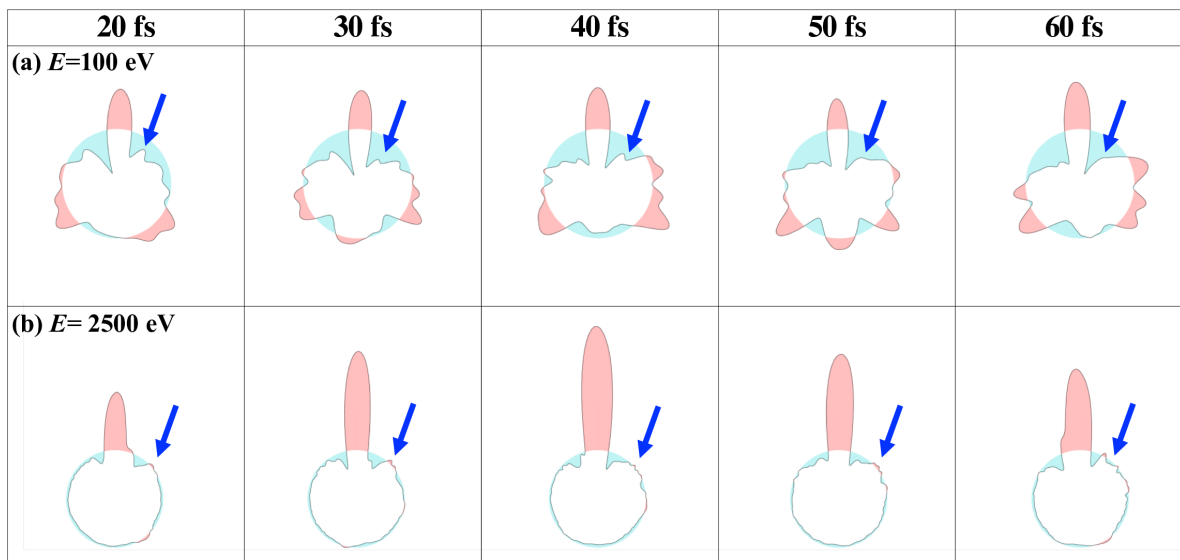


**Fig. 4** Snapshots of PA-MFPADs averaged over 15 trajectories for  $\text{H}_3^+$  generation (from 20 to 60 fs) at photoelectron energies (a) 100 eV and (b) 2.5 keV. The blue arrows indicate the position of the peak associated with  $\text{H}_3^+$  in each time frame.

patible with the evolution of the corresponding  $\text{OH}_2^+$  and  $\text{OH}_3^+$  yields with time (see Supplementary Information) and are similar to those reported in previous IR pump - IR probe CEI experiments<sup>22</sup>.

We now examine if a similar approach can also provide an intuitive dynamical picture in a much more complex scenario, hydrogen roaming, for which real-time observations have only been reported very recently by using CEI in combination with sophisticated quantum mechanical calculations<sup>23</sup>. This process involves the motion of three hydrogen atoms and it is, therefore, much more challenging to identify. As mentioned above, in this case we use the reaction plane defined by the momentum correlations between  $\text{H}_{\text{mig}}^+$ ,  $\text{C}_2\text{H}_2^+$  (or the sum of  $\text{CH}_m^+$  and  $\text{CH}_n^+$  with  $m+n=2$ ) and the sum of  $\text{O}^+$  and  $\text{H}^+$  (or  $\text{OH}^+$ ). Fig. 4 shows the calculated PA-MFPADs obtained as the average of the PA-MFPADs for all individual trajectories leading to  $\text{H}_3^+$ . As can be seen,  $\text{H}_3^+$  formation leads to tiny, but still visible structures in the PA-MFPADs at low and high photoelectron energies. Changes in these structures are also visible, although much less pronounced than for single- and double-hydrogen migration, so that it is very difficult to go into the details of the roaming dynamics. This is due to the fact that O 1s ionization occurs rather far away from the region where  $\text{H}_{\text{mig}}^+$  is ejected to meet the previously formed  $\text{H}_2$  molecule. C(1s) ionization by the probe pulse would be probably a better option to observe the dynamics due to the proximity of both carbon atoms to the region of interest. However, the analysis of the measured PA-MFPADs would probably be more cumbersome due to the likely presence of two-center interferences associated with the ionization of the two neighboring atoms.

## 4 Conclusions

In conclusion, by combining molecular dynamics and electron scattering methods, we have shown that time- and momentum-resolved photoelectron diffraction (TMR-PED) allows for a direct imaging of single- and double-hydrogen migration in doubly-

charged ethanol with few-fs temporal and Å spatial resolutions, all the way until the end of the process. The same procedure can also provide evidence of the more involved hydrogen roaming process. The signature of the moving hydrogen atoms can be clearly seen in polarization-averaged molecular-frame photoelectron angular distributions (PA-MFPADs), in which the positions of several structures (either peaks or depletions) change with time following the trajectory of those atoms. Thus, the motion of these structures provides a straightforward connection with the dynamics of hydrogen migration in real space. Measuring TMR-PED has now become feasible by using XFEL pulses due to their high repetition-rate and ultrashort duration (few- down to sub-fs), which can thus be efficiently combined with multi-coincidence detection techniques such as COLTRIMS. Therefore, TMR-PED is expected to provide unprecedented insight on hydrogen migration process in the very near future.

## Conflicts of interest

There are no conflicts to declare’.

## Acknowledgements

This work was performed under the European COST Action CA18222 AttoChem and Cooperative Research Program of “Network Joint Research Center for Materials and Devices.” K.H. acknowledges funding by JSPS KAKENHI under Grant No. 18K05027 and 17K04980. This work was partially funded by the Spanish Ministry of Science and Innovation – Ministerio Español de Ciencia e Innovación MICINN – projects PID2019-105458RB-I00 and PID2019-110091GB-I00, the Severo Ochoa Programme for Centres of Excellence in R & D (SEV-2016-0686) and the María de Maeztu Programme for Units of Excellence in R & D (CEX2018-000805-M). We acknowledge the generous allocation of computer time at the Centro de Computación Científica at the Universidad Autónoma de Madrid (CCC-UAM).

## Notes and references

- 1 A. H. Zewail, *4D visualization of matter: recent collected works*, Imperial College Press, London, 2014.
- 2 R. D. Miller, *Annual Review of Physical Chemistry*, 2014, **65**, 583–604.
- 3 F. Krausz and M. Ivanov, *Rev. Mod. Phys.*, 2009, **81**, 163–234.
- 4 E. Lindroth, F. Calegari, L. Young, M. Harmand, N. Dudovich, N. Berrah and O. Smirnova, *Nature Reviews Physics*, 2019, **1**, 107–111.
- 5 J. Li, J. Lu, A. Chew, S. Han, J. Li, Y. Wu, H. Wang, S. Ghimire and Z. Chang, *Nature Communications*, 2020, **11**, 2748.
- 6 P. Emma, R. Akre, J. Arthur, R. Bionta, C. Bostedt, J. Bozek, A. Brachmann, P. Bucksbaum, R. Coffee, F.-J. Decker, Y. Ding, D. Dowell, S. Edstrom, A. Fisher, J. Frisch, S. Gilevich, J. Hastings, G. Hays, P. Hering, Z. Huang, R. Iverson, H. Loos, M. Messerschmidt, A. Miahnahri, S. Moeller, H.-D. Nuhn, G. Pile, D. Ratner, J. Rzepiela, D. Schultz, T. Smith, P. Stefan, H. Tompkins, J. Turner, J. Welch, W. White, J. Wu, G. Yocky and J. Galayda, *Nature Photonics*, 2010, **4**, 641–647.
- 7 S. P. Weathersby, G. Brown, M. Centurion, T. F. Chase, R. Coffee, J. Corbett, J. P. Eichner, J. C. Frisch, A. R. Fry, M. Gühr, N. Hartmann, C. Hast, R. Hettel, R. K. Jobe, E. N. Jongewaard, J. R. Lewandowski, R. K. Li, A. M. Lindenberg, I. Makasyuk, J. E. May, D. McCormick, M. N. Nguyen, A. H. Reid, X. Shen, K. Sokolowski-Tinten, T. Vecchione, S. L. Vetter, J. Wu, J. Yang, H. A. Dürr and X. J. Wang, *Review of Scientific Instruments*, 2015, **86**, 073702.
- 8 T. J. A. Wolf, D. M. Sanchez, J. Yang, R. M. Parrish, J. P. F. Nunes, M. Centurion, R. Coffee, J. P. Cryan, M. Gühr, K. Hegazy, A. Kirrander, R. K. Li, J. Ruddock, X. Shen, T. Vecchione, S. P. Weathersby, P. M. Weber, K. Wilkin, H. Yong, Q. Zheng, X. J. Wang, M. P. Minitti and T. J. Martínez, *Nature Chemistry*, 2019, **11**, 504 – 509.
- 9 M. P. Minitti, J. M. Budarz, A. Kirrander, J. S. Robinson, D. Ratner, T. J. Lane, D. Zhu, J. M. Glownia, M. Kozina, H. T. Lemke, M. Sikorski, Y. Feng, S. Nelson, K. Saita, B. Stankus, T. Northey, J. B. Hastings and P. M. Weber, *Phys. Rev. Lett.*, 2015, **114**, 255501.
- 10 T. Kierspel, A. Morgan, J. Wiese, T. Mullins, A. Aquila, A. Barty, R. Bean, R. Boll, S. Boutet, P. Bucksbaum, H. N. Chapman, L. Christensen, A. Fry, M. Hunter, J. E. Koglin, M. Liang, V. Mariani, A. Natan, J. Robinson, D. Rolles, A. Rudenko, K. Schnorr, H. Stapelfeldt, S. Stern, J. Thøgersen, C. H. Yoon, F. Wang and J. Küpper, *The Journal of Chemical Physics*, 2020, **152**, 084307.
- 11 A. Barty, *Current Opinion in Structural Biology*, 2016, **40**, 186–194.
- 12 P. K. Horan and W. Snipes, *International Journal of Radiation Biology and Related Studies in Physics, Chemistry and Medicine*, 1970, **17**, 201–203.
- 13 S. W. Englander and M. M. G. Krishna, *Nature Structural Biology*, 2001, **8**, 741–742.
- 14 K. D. Rand, C. M. Adams, R. A. Zubarev and T. J. D. Jäyrgensen, *Journal of the American Chemical Society*, 2008, **130**, 1341–1349.
- 15 A. Ledvina, G. McAlister, M. Gardner, S. Smith, J. Madsen, J. Schwartz, G. Stafford Jr., J. Syka, J. Brodbelt and J. Coon, *Angewandte Chemie International Edition*, 2009, **48**, 8526–8528.
- 16 J. Zhao, T. Song, M. Xu, Q. Quan, K. W. M. Siu, A. C. Hopkinson and I. K. Chu, *Phys. Chem. Chem. Phys.*, 2012, **14**, 8723–8731.
- 17 A. Hishikawa, A. Matsuda, M. Fushitani and E. J. Takahashi, *Physical Review Letters*, 2007, **99**, 258302.
- 18 Y. H. Jiang, A. Rudenko, O. Herrwerth, L. Foucar, M. Kurka, K. U. Kühnel, M. Lezius, M. F. Kling, J. van Tilborg, A. Belkacem, K. Ueda, S. Düsterer, R. Treusch, C. D. Schröter, R. Moshhammer and J. Ullrich, *Physical Review Letters*, 2010, **105**, 263002.
- 19 H. Ibrahim, B. Wales, S. Beaulieu, B. E. Schmidt, N. Thiré, E. P. Fowe, É. Bisson, C. T. Hebeisen, V. Wanie, M. Giguère, J.-C. Kieffer, M. Spanner, A. D. Bandrauk, J. Sanderson, M. S. Schuurman and F. Légaré, *Nature Communications*, 2014, **5**, 4422.
- 20 C. E. Liekhus-Schmaltz, I. Tenney, T. Osipov, A. Sanchez-Gonzalez, N. Berrah, R. Boll, C. Bomme, C. Bostedt, J. D. Bozek, S. Carron, R. Coffee, J. Devin, B. Erk, K. R. Ferguson, R. W. Field, L. Foucar, L. J. Frasinski, J. M. Glownia, M. Gühr, A. Kamalov, J. Krzywinski, H. Li, J. P. Marangos, T. J. Martinez, B. K. McFarland, S. Miyabe, B. Murphy, A. Natan, D. Rolles, A. Rudenko, M. Siano, E. R. Simpson, L. Spector, M. Swiggers, D. Walke, S. Wang, T. Weber, P. H. Bucksbaum and V. S. Petrovic, *Nature Communications*, 2015, **6**, 8199.
- 21 M. McDonnell, A. C. LaForge, J. Reino-González, M. Disla, N. G. Kling, D. Mishra, R. Obaid, M. Sundberg, V. Svoboda, S. Díaz-Tendero, F. Martín and N. Berrah, *The Journal of Physical Chemistry Letters*, 2020, **11**, 6724–6729.
- 22 N. G. Kling, S. Díaz-Tendero, R. Obaid, M. R. Disla, H. Xiong, M. Sundberg, S. D. Khosravi, M. Davino, P. Drach, A. M. Carroll, T. Osipov, F. Martín and N. Berrah, *Nature Communications*, 2019, **10**, 2813.
- 23 T. Endo, S. P. Neville, V. Wanie, S. Beaulieu, C. Qu, J. Deschamps, P. Lassonde, B. E. Schmidt, H. Fujise, M. Fushitani, A. Hishikawa, P. L. Houston, J. M. Bowman, M. S. Schuurman, F. Légaré and H. Ibrahim, *Science*, 2020, **370**, 1072–1077.
- 24 C. I. Blaga, J. Xu, A. D. Di Chiara, E. Sistrunk, K. Zhang, P. Agostini, T. A. Miller, L. F. Di Mauro and C. D. Lin, *Nature*, 2012, **483**, 194–197.
- 25 A. Sanchez, K. Amini, S.-J. Wang, T. Steinle, B. Belsa, J. Danek, A. T. Le, X. Liu, R. Moshhammer, T. Pfeifer, M. Richter, J. Ullrich, S. Gräfe, C. D. Lin and J. Biegert, *Nature Communications*, 2021, **12**, 1520.
- 26 X. Liu, K. Amini, T. Steinle, A. Sanchez, M. Shaikh, B. Belsa, J. Steinmetzer, A.-T. Le, R. Moshhammer, T. Pfeifer, J. Ullrich, R. Moszynski, C. D. Lin, S. Gräfe and J. Biegert, *The Journal of Chemical Physics*, 2019, **151**, 024306.
- 27 B. Wolter, M. G. Pullen, A.-T. Le, M. Baudisch, K. Doblhoff-Dier, A. Senftleben, M. Hemmer, C. D. Schröter, J. Ullrich, T. Pfeifer, R. Moshhammer, S. Gräfe, O. Vendrell, C. D. Lin and



- J. Biegert, *Science*, 2016, **354**, 308–312.
- 28 E. Pléziat, L. Argenti, E. Kuk, C. Miron, K. Ueda, P. Decleva and F. Martín, *Phys. Rev. A*, 2012, **85**, 023409.
  - 29 S. Nandi, E. Pléziat, M. Patanen, C. Miron, J. D. Bozek, F. Martin, D. Toffoli and P. Decleva, *Phys. Chem. Chem. Phys.*, 2016, **18**, 3214–3222.
  - 30 S. Engin, J. Gonzalez-Vazquez, G. G. Maliyar, A. R. Milosavljević, T. Ono, S. Nandi, D. Iablonskyi, K. Kooser, J. D. Bozek, P. Decleva, E. Kuk, K. Ueda and F. Martin, *Structural Dynamics*, 2019, **6**, 054101.
  - 31 D. P. Woodruff, *Applied Physics A*, 2008, **92**, 439–445.
  - 32 J. Ullrich, R. Moshhammer, A. Dorn, R. Dörner, L. P. H. Schmidt and H. Schmidt-Böcking, *Reports on Progress in Physics*, 2003, **66**, 1463–1545.
  - 33 F. Krasniqi, B. Najjari, L. Strüder, D. Rolles, A. Voitkiv and J. Ullrich, *Physical Review A*, 2010, **81**, 033411.
  - 34 M. Kazama, T. Fujikawa, N. Kishimoto, T. Mizuno, J.-i. Adachi and A. Yagishita, *Physical Review A*, 2013, **87**, 063417.
  - 35 A. Rouzée, P. Johnsson, L. Rading, A. Hundertmark, W. Siu, Y. Huismans, S. Düsterer, H. Redlin, F. Tavella, N. Stojanovic, A. Al-Shemmary, F. Lépine, D. M. P. Holland, T. Schlatholter, R. Hoekstra, H. Fukuzawa, K. Ueda and M. J. J. Vrakking, *Journal of Physics B: Atomic, Molecular and Optical Physics*, 2013, **46**, 164029.
  - 36 W. Decking, S. Abeghyan, P. Abramian, A. Abramsky, A. Aguirre, C. Albrecht, P. Alou, M. Altarelli, P. Altmann, K. Amyan, V. Anashin, E. Apostolov, K. Appel, D. Augustine, V. Ayvazyan, S. Baark, F. Babies, N. Baboi, P. Bak, V. Balandin, R. Baldinger, B. Baranasic, S. Barbanotti, O. Belikov, V. Belokurov, L. Belova, V. Belyakov, S. Berry, M. Bertucci, B. Beutner, A. Block, M. Blöcher, T. Böckmann, C. Bohm, M. Böhnert, V. Bondar, E. Bondarchuk, M. Bonezzi, P. Borowiec, C. Bösch, U. Bösenberg, A. Bosotti, R. Böspflug, M. Bousonville, E. Boyd, Y. Bozhko, A. Brand, J. Branlard, S. Briechele, F. Brinker, S. Brinker, R. Brinkmann, S. Brockhauser, O. Brovko, H. Brück, A. Brüdgam, L. Butkowski, T. Büttner, J. Calero, E. Castro-Carballo, G. Cattalanotto, J. Charrier, J. Chen, A. Cherepenko, V. Cheskidov, M. Chiodini, A. Chong, S. Choroba, M. Chorowski, D. Churanov, W. Cichalewski, M. Clausen, W. Clement, C. Cloué, J. A. Cobos, N. Coppola, S. Cunis, K. Czuba, M. Czwalińska, B. D’Almagne, J. Dammann, H. Danared, A. de Zubiaurre Wagner, A. Delfs, T. Delfs, F. Dietrich, T. Dietrich, M. Dohlus, M. Dommach, A. Donat, X. Dong, N. Doynikov, M. Dressel, M. Duda, P. Duda, H. Eckoldt, W. Ehsan, J. Eidam, F. Eints, C. Engling, U. Englisch, A. Ermakov, K. Escherich, J. Eschke, E. Saldin, M. Faesing, A. Fallou, M. Felber, M. Fenner, B. Fernandes, J. M. Fernández, S. Feuker, K. Filippakopoulos, K. Floettmann, V. Fogel, M. Fontaine, A. Francés, I. F. Martin, W. Freund, T. Freyermuth, M. Friedland, L. Fröhlich, M. Fusetti, J. Fydrych, A. Gallas, O. García, L. Garcia-Tabares, G. Geloni, N. Gerasimova, C. Gerth, P. Geßler, V. Gharibyan, M. Gloor, J. Głowinkowski, A. Goesel, Z. Gołębiewski, N. Golubeva, W. Grabowski, W. Graeff, A. Grebentsov, M. Grecki, T. Grevsmuehl, M. Gross, U. Grosse-Wortmann, J. Grünert, S. Grunewald, P. Grzegory, G. Feng, H. Guler, G. Gusev, J. L. Gutierrez, L. Hagge, M. Hamberg, R. Hanneken, E. Harms, I. Hartl, A. Hauberg, S. Hauf, J. Hauschildt, J. Hauser, J. Havlicek, A. Hedqvist, N. Heidbrook, F. Hellberg, D. Henning, O. Hensler, T. Hermann, A. Hidvégi, M. Hierholzer, H. Hintz, F. Hoffmann, M. Hoffmann, M. Hoffmann, Y. Holler, M. Hüning, A. Ignatenko, M. Ilchen, A. Iluk, J. Iversen, J. Iversen, M. Izquierdo, L. Jachmann, N. Jardon, U. Jastrow, K. Jenssch, J. Jensen, M. Ježabek, M. Jidda, H. Jin, N. Johansson, R. Jonas, W. Kaabi, D. Kaefler, R. Kammering, H. Kapitza, S. Karabekyan, S. Karstensen, K. Kasprzak, V. Katalev, D. Keese, B. Keil, M. Kholopov, M. Killenberger, B. Kitaev, Y. Klimchenko, R. Klos, L. Knebel, A. Koch, M. Koepke, S. Köhler, W. Köhler, N. Kohlstrunk, Z. Konopkova, A. Konstantinov, W. Kook, W. Koprek, M. Körfer, O. Korth, A. Kosarev, K. Kosiński, D. Kostin, Y. Kot, A. Kotarba, T. Kozak, V. Kozak, R. Kramert, M. Krasilnikov, A. Krasnov, B. Krause, L. Kravchuk, O. Krebs, R. Kretschmer, J. Kreutzkamp, O. Kröplin, K. Krzysik, G. Kube, H. Kuehn, N. Kujala, V. Kulikov, V. Kuzminych, D. L. Civita, M. Lacroix, T. Lamb, A. Lancetov, M. Larsson, D. L. Pinvidic, S. Lederer, T. Lensch, D. Lenz, A. Leuschner, F. Levenhagen, Y. Li, J. Liebing, L. Lilje, T. Limberg, D. Lipka, B. List, J. Liu, S. Liu, B. Lorbeer, J. Lorkiewicz, H. H. Lu, F. Ludwig, K. Machau, W. Maciocha, C. Madec, C. Magueur, C. Maiano, I. Maksimova, K. Malcher, T. Maltezopoulos, E. Mamoshkina, B. Manschwetus, F. Marcellini, G. Marinkovic, T. Martinez, H. Martirosyan, W. Maschmann, M. Maslov, A. Matheisen, U. Mavric, J. Meißner, K. Meissner, M. Messerschmidt, N. Meyners, G. Michalski, P. Michelato, N. Mildner, M. Moe, F. Moglia, C. Mohr, S. Mohr, W. Möller, M. Mommerz, L. Monaco, C. Montiel, M. Moretti, I. Morozov, P. Morozov, D. Mross, J. Mueller, C. Müller, J. Müller, K. Müller, J. Munilla, A. Münich, V. Muratov, O. Napoly, B. Näser, N. Nefedov, R. Neumann, R. Neumann, N. Ngada, D. Noelle, F. Obier, I. Okunev, J. A. Oliver, M. Omet, A. Oppelt, A. Ottmar, M. Oublaïd, C. Pagani, R. Paparella, V. Paramonov, C. Peitzmann, J. Penning, A. Perus, F. Peters, B. Petersen, A. Petrov, I. Petrov, S. Pfeiffer, J. Pflüger, S. Philipp, Y. Pienaud, P. Pierini, S. Pivovarov, M. Planas, E. Pławski, M. Pohl, J. Polinski, V. Popov, S. Prat, J. Prenting, G. Priebe, H. Pryschelski, K. Przygoda, E. Pyata, B. Racky, A. Rathjen, W. Ratuschni, S. Regnaud-Campderros, K. Rehlich, D. Reschke, C. Robson, J. Roever, M. Roggli, J. Rothenburg, E. Rusiński, R. Rybaniec, H. Sahling, M. Salmani, L. Samoylova, D. Sanzone, F. Saretzki, O. Sawlanski, J. Schaffran, H. Schlarb, M. Schlösser, V. Schlott, C. Schmidt, F. Schmidt-Foehre, M. Schmitz, M. Schmökel, T. Schnautz, E. Schneidmiller, M. Scholz, B. Schöneburg, J. Schultze, C. Schulz, A. Schwarz, J. Sekutowicz, D. Sellmann, E. Semenov, S. Serkez, D. Sertore, N. Shehzad, P. Shemarykin, L. Shi, M. Sienkiewicz, D. Sikora, M. Sikorski, A. Silenzi, C. Simon, W. Singer, X. Singer, H. Sinn, K. Sinram, N. Skvorodnev, P. Smirnow, T. Sommer, A. Sorokin, M. Stadler, M. Steckel, B. Steffen, N. Steinhau-Kühl, F. Stephan, M. Stodulski, M. Stolper, A. Sulimov, R. Susen, J. Świerblewski, C. Sydlo, E. Syresin, V. Sytchev,

- J. Szuba, N. Tesch, J. Thie, A. Thiebault, K. Tiedtke, D. Tischhauser, J. Tolkiehn, S. Tomin, F. Tonisch, F. Toral, I. Torbin, A. Trapp, D. Treyer, G. Trowitzsch, T. Trublet, T. Tschentscher, F. Ullrich, M. Vannoni, P. Varela, G. Varghese, G. Vashchenko, M. Vasic, C. Vazquez-Velez, A. Verguet, S. Vilcins-Czvitkovits, R. Villanueva, B. Visentin, M. Viti, E. Vogel, E. Volobuev, R. Wagner, N. Walker, T. Wamsat, H. Weddig, G. Weichert, H. Weise, R. Wennendorf, M. Werner, R. Wichmann, C. Wiebers, M. Wiencek, T. Wilksen, I. Will, L. Winkelmann, M. Winkowski, K. Wittenburg, A. Witzig, P. Wlk, T. Wohlenberg, M. Wojciechowski, F. Wolff-Fabris, G. Wrochna, K. Wrona, M. Yakopov, B. Yang, F. Yang, M. Yurkov, I. Zagorodnov, P. Zalden, A. Zavadtsev, D. Zavadtsev, A. Zhirnov, A. Zhukov, V. Ziemann, A. Zolotov, N. Zolotukhina, F. Zummack and D. Zybin, *Nature Photonics*, 2020, **14**, 391–397.
- 37 J. Duris, S. Li, T. Driver, E. G. Champenois, J. P. MacArthur, A. A. Lutman, Z. Zhang, P. Rosenberger, J. W. Aldrich, R. Coffee, G. Coslovich, F.-J. Decker, J. M. Glowina, G. Hartmann, W. Helml, A. Kamalov, J. Knurr, J. Krzywinski, M.-F. Lin, J. P. Marangos, M. Nantel, A. Natan, J. T. O’Neal, N. Shivaram, P. Walter, A. L. Wang, J. J. Welch, T. J. A. Wolf, J. Z. Xu, M. F. Kling, P. H. Bucksbaum, A. Zholents, Z. Huang, J. P. Cryan and A. Marinelli, *Nature Photonics*, 2020, **14**, 30–36.
- 38 G. Kastirke, M. S. Schöffler, M. Weller, J. Rist, R. Boll, N. Anders, T. M. Baumann, S. Eckart, B. Erk, A. De Fanis, K. Fehre, A. Gatton, S. Grundmann, P. Grychtol, A. Hartung, M. Hofmann, M. Ilchen, C. Janke, M. Kircher, M. Kunitski, X. Li, T. Mazza, N. Melzer, J. Montano, V. Music, G. Nalin, Y. Ovcharenko, A. Pier, N. Rennhack, D. E. Rivas, R. Dörner, D. Rolles, A. Rudenko, P. Schmidt, J. Siebert, N. Strenger, D. Trabert, I. Vela-Perez, R. Wagner, T. Weber, J. B. Williams, P. Ziolkowski, L. P. H. Schmidt, A. Czasch, F. Trinter, M. Meyer, K. Ueda, P. V. Demekhin and T. Jahnke, *Physical Review X*, 2020, **10**, 021052.
- 39 G. Kastirke, M. S. Schöffler, M. Weller, J. Rist, R. Boll, N. Anders, T. M. Baumann, S. Eckart, B. Erk, A. De Fanis, K. Fehre, A. Gatton, S. Grundmann, P. Grychtol, A. Hartung, M. Hofmann, M. Ilchen, C. Janke, M. Kircher, M. Kunitski, X. Li, T. Mazza, N. Melzer, J. Montano, V. Music, G. Nalin, Y. Ovcharenko, A. Pier, N. Rennhack, D. E. Rivas, R. Dörner, D. Rolles, A. Rudenko, P. Schmidt, J. Siebert, N. Strenger, D. Trabert, I. Vela-Perez, R. Wagner, T. Weber, J. B. Williams, P. Ziolkowski, L. P. H. Schmidt, A. Czasch, K. Ueda, F. Trinter, M. Meyer, P. V. Demekhin and T. Jahnke, *Phys. Rev. Lett.*, 2020, **125**, 163201.
- 40 S. Serkez, W. Decking, L. Froehlich, N. Gerasimova, J. Grüntert, M. Guetg, M. Huttula, S. Karabekyan, A. Koch, V. Kocharyan and et al., *Applied Sciences*, 2020, **10**, 2728.
- 41 H. B. Schlegel, J. M. Millam, S. S. Iyengar, G. A. Voth, A. D. Daniels, G. E. Scuseria and M. J. Frisch, *J. Chem. Phys.*, 2001, **114**, 9758–9763.
- 42 S. S. Iyengar, H. B. Schlegel, J. M. Millam, G. A. Voth, G. E. Scuseria and M. J. Frisch, *J. Chem. Phys.*, 2001, **115**, 10291–10302.
- 43 H. B. Schlegel, S. S. Iyengar, X. Li, J. M. Millam, G. A. Voth, G. E. Scuseria and M. J. Frisch, *J. Chem. Phys.*, 2002, **117**, 8694–8704.
- 44 A. D. Becke, *The Journal of Chemical Physics*, 1993, **98**, 5648–5652.
- 45 C. Lee, W. Yang and R. G. Parr, *Phys. Rev. B*, 1988, **37**, 785–789.
- 46 B. Miehlich, A. Savin, H. Stoll and H. Preuss, *Chemical Physics Letters*, 1989, **157**, 200 – 206.
- 47 T. Clark, J. Chandrasekhar, G. W. Spitznagel and P. Von Raguë Schleyer, *J. Comput. Chem.*, 1983, **4**, 294–301.
- 48 P. C. Hariharan and J. A. Pople, *Theor. Chim. Acta*, 1973, **28**, 213–222.
- 49 W. J. Hehre, R. Ditchfield and J. A. Pople, *J. Chem. Phys.*, 1972, **56**, 2257–2261.
- 50 G. D. Purvis and R. J. Bartlett, *The Journal of Chemical Physics*, 1982, **76**, 1910–1918.
- 51 J. A. Pople, M. Head-Gordon and K. Raghavachari, *The Journal of Chemical Physics*, 1987, **87**, 5968–5975.
- 52 T. H. Dunning, *J. Chem. Phys.*, 1989, **90**, 1007–1023.
- 53 R. A. Kendall, T. H. Dunning and R. J. Harrison, *J. Chem. Phys.*, 1992, **96**, 6796–6806.
- 54 M. J. Frisch, G. W. Trucks, H. B. Schlegel, G. E. Scuseria, M. A. Robb, J. R. Cheeseman, G. Scalmani, V. Barone, G. A. Petersson, H. Nakatsuji, X. Li, M. Caricato, A. V. Marenich, J. Bloino, B. G. Janesko, R. Gomperts, B. Mennucci, H. P. Hratchian, J. V. Ortiz, A. F. Izmaylov, J. L. Sonnenberg, D. Williams-Young, F. Ding, F. Lipparini, F. Egidi, J. Goings, B. Peng, A. Petrone, T. Henderson, D. Ranasinghe, V. G. Zakrzewski, J. Gao, N. Rega, G. Zheng, W. Liang, M. Hada, M. Ehara, K. Toyota, R. Fukuda, J. Hasegawa, M. Ishida, T. Nakajima, Y. Honda, O. Kitao, H. Nakai, T. Vreven, K. Throssell, J. A. Montgomery, Jr., J. E. Peralta, F. Ogliaro, M. J. Bearpark, J. J. Heyd, E. N. Brothers, K. N. Kudin, V. N. Staroverov, T. A. Keith, R. Kobayashi, J. Normand, K. Raghavachari, A. P. Rendell, J. C. Burant, S. S. Iyengar, J. Tomasi, M. Cossi, J. M. Millam, M. Klene, C. Adamo, R. Cammi, J. W. Ochterski, R. L. Martin, K. Morokuma, O. Farkas, J. B. Foresman and D. J. Fox, *Gaussian 16 Revision C.01*, 2016, Gaussian Inc. Wallingford CT.
- 55 C. R. Natoli, M. Benfatto, S. Della Longa and K. Hatada, *Journal of Synchrotron Radiation*, 2003, **10**, 26–42.
- 56 J. Desclaux, *Computer Physics Communications*, 1975, **9**, 31 – 45.
- 57 L. Hedin and S. Lundqvist, *S. Lundqvist*, Academic Press, 1970, vol. 23, pp. 1 – 181.
- 58 L. Hedin and B. I. Lundqvist, *Journal of Physics C: Solid State Physics*, 1971, **4**, 2064–2083.
- 59 J. G. Norman, *Molecular Physics*, 1976, **31**, 1191–1198.
- 60 F. Ota, K. Yamazaki, D. Sébilleau, K. Ueda and K. Hatada, *Journal of Physics B: Atomic, Molecular and Optical Physics*, 2021, **54**, 024003.
- 61 D. Sébilleau, C. Natoli, G. M. Gavaza, H. Zhao, F. Da Pieve and K. Hatada, *Computer Physics Communications*, 2011, **182**,

2567 – 2579.

- 62 J. B. Williams, C. S. Trevisan, M. S. Schöffler, T. Jahnke, I. Bocharova, H. Kim, B. Ulrich, R. Wallauer, F. Sturm, T. N. Rescigno, A. Belkacem, R. Dörner, T. Weber, C. W. McCurdy and A. L. Landers, *Physical Review Letters*, 2012, **108**, 233002.
- 63 E. Plésiat, P. Decleva and F. Martín, *Phys. Rev. A*, 2013, **88**,

063409.

- 64 H. Fukuzawa, R. R. Lucchese, X.-J. Liu, K. Sakai, H. Iwayama, K. Nagaya, K. Kreidi, M. S. Schöffler, J. R. Harries, Y. Tamenori, Y. Morishita, I. H. Suzuki, N. Saito and K. Ueda, *The Journal of Chemical Physics*, 2019, **150**, 174306.